EUROPEAN JOURNAL OF PURE AND APPLIED MATHEMATICS
2025, Vol. 18, Issue 1, Article Number 5502
ISSN 1307-5543 – ejpam.com
Published by New York Business Global

Heat Transfer and Magnetohydrodynamic Nanofluid Flow Caused by a Stretching Sheet Heated Convectively: Numerical Investigation

M. Adel[1,*], M. M. Khader[2,3], M. M. Babatin[2], I. Alraddadi[1], A. Alaidrous[4], G. M. Ismail[1]

[1] *Department of Mathematics, Faculty of Science, Islamic University of Madinah, Medina, Saudi Arabia*
[2] *Department of Mathematics and Statistics, College of Science, Imam Mohammad Ibn Saud Islamic University (IMSIU), Riyadh, Saudi Arabia*
[3] *Department of Mathematics, Faculty of Science, Benha University, Benha, Egypt*
[4] *Mathematics Department, Faculty of Sciences, Umm Al-Qura University, Makkah, Saudi Arabia*

Abstract. This paper describes a new study that looks at how a magnetohydrodynamic (MHD) nanofluid moves and transfers heat over a porous medium with a stretched sheet that moves in a straight line. This study investigates the effects of heat radiation, viscous dissipation, and convective boundary conditions (CBCs) on the dynamics of nanofluids, an area that has received insufficient exploration despite its significance in both commercial and scientific contexts. The research formulates the fundamental conservation equations for mass, momentum, heat, and nanoparticle concentration, which are transformed from nonlinear PDEs into a system of ODEs. These equations are solved numerically using the Hermite collocation method (HCM), with results visualized to illustrate the impact of key physical parameters. This work has practical applications in fields such as cooling technologies, energy systems, and materials engineering, where enhanced thermal management and precise control over nanofluid properties are crucial for performance optimization.

2020 Mathematics Subject Classifications: 41A30, 76F12, 65M60, 65N12
Key Words and Phrases: Nanofluid, Convective CBCs, Slip impacts, Thermal radiation, HCM

1. Introduction

It is very important in engineering and other fields of industry to study boundary BL phenomena that involve fluid flow and heat transfer from surfaces that are moving

*Corresponding author.
DOI: https://doi.org/10.29020/nybg.ejpam.v18i1.5502

Email addresses: m.adel@iu.edu.sa and adel@sci.cu.edu.eg (M. Adel), mmkhader@imamu.edu.sa (M. M. Khader), mmbabatin@imamu.edu.sa (M. M. Babatin), ialraddadi@iu.edu.sa (I. Alraddadi), aaaidrous@uqu.edu.sa (A. Alaidrous), gamalm2010@yahoo.com (G. M. Ismail)

or stretching. This study domain has substantial applicability across various industries, including but not limited to extrusion, wire drawing, and massive metallic plates utilized in electrolyte systems and cooling. This study is the first to look at how a magnetohydrodynamic (MHD) nanofluid flows and transfers heat over porous media with a stretched sheet that moves in a straight line. This study specifically investigates the effects of heat radiation, viscous dissipation, and convective CBCs on nanofluid behavior, an area that has received insufficient research despite its significance in both commercial and scientific domains [6].

Nanoparticles refer to particulate matter ranging from 1 to 100 nanometers in size. Nanofluids are generated by scattering nanoparticles inside a base fluid. This category of fluid exhibits an innovative domain of nanotechnology aimed at enhancing thermal conductivity. Progress in nanofluid technology has produced materials with markedly enhanced thermal conductivity and superior heat transfer properties. Choi [5] undertook a comprehensive investigation of nanoparticles, leading the inquiry in this domain and establishing himself as the first contributor to this area of research. Further, nanofluids also significantly enhance mass transfer, impacting areas like drug delivery, biomedical devices, and renewable energy ([10], [21]). Customized models accounting for non-Newtonian behavior, viscous dissipation, and slip effects provide precise adaptability, proving valuable in various industrial and technological applications.

Generally considered negligible, viscous dissipation can exert a considerable influence in instances of exceptionally high fluid viscosity. Variations in temperature distribution influence the rate of heat transfer ([1], [19], [23]). Viscous dissipation is essential since it converts mechanical energy into thermal energy in viscous fluids.

The Hermite collocation method is an effective strategy for solving various problems, as evidenced by its application in numerous studies, including those referenced in papers such as ([4], [17], [15]). Consequently, we employ this method as a numerical solution to tackle the presented problem. The Hermite collocation technique is essential in numerical analysis and mathematical modeling due to its accuracy, adaptability in addressing boundary value problems, and efficacy in dealing with singularities. Its capacity to deliver accurate solutions to DEs makes it a versatile tool useful in numerous scientific and technical fields. Its significance lies in its ability to contribute to the attainment of stable and precise numerical solutions, particularly in situations involving intricate phenomena and problems with specified conditions at both ends of the domain ([14], [16]).

As per the author's current understanding, this specific feature is not covered in the existing literature. The aim of examining these studies on lubricated Newtonian nanofluids is to offer a precise portrayal of the nanofluid's transport properties. The analysis examines the impact of thermal radiation, viscous dissipation, and CBCs. The HCM is employed to graphically illustrate the impacts of these features.

2. Methodology

Assume the existence of a continuous, smooth-flowing, and incompressible nanofluid in the region where y is greater than zero. This fluid originates from a permeable solid

surface at $y = 0$, with the reference point clearly marked at $x = 0$ in Figure 1.

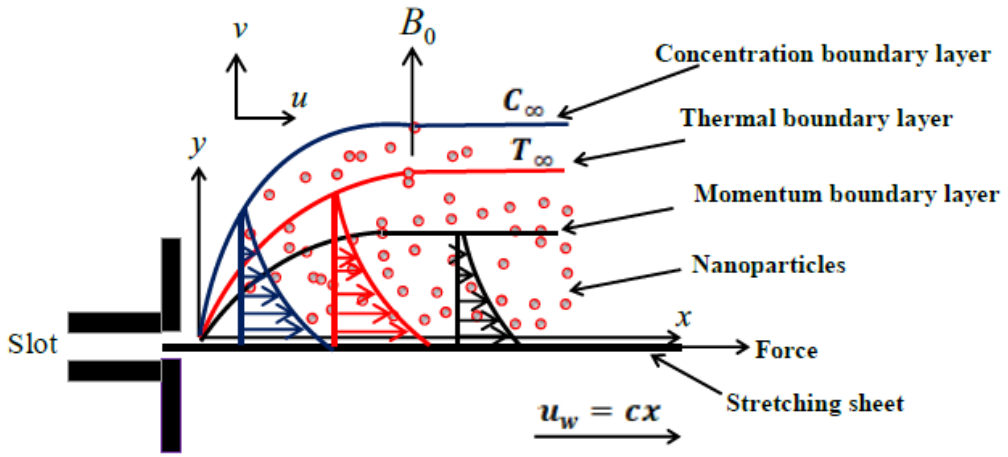

Figure 1. Schematic diagram of the model

A slender solid surface projects from a slit at the origin and experiences extension in the x-direction. The initial circumstances yield the constitutive equations for the nanofluid model in this format [22]:

$$\nabla.(u, v) = 0, \tag{1}$$

$$(u, v).\nabla\, u = \frac{\mu}{\rho}\frac{\partial^2 u}{\partial y^2} - \frac{\sigma B_0^2}{\rho}u, \tag{2}$$

$$(u, v).\nabla\, T = \frac{\kappa}{\rho c_p}\left(\frac{\partial^2 T}{\partial y^2}\right) + \frac{\mu}{\rho c_p}\left(\frac{\partial u}{\partial y}\right)^2 - \frac{1}{\rho c_p}\frac{\partial q_r}{\partial y} + \tau\left(D_B\frac{\partial C}{\partial y}\frac{\partial T}{\partial y} + \frac{D_T}{T_\infty}\left(\frac{\partial T}{\partial y}\right)^2\right), \tag{3}$$

$$(u, v).\nabla\, C = D_B\left(\frac{\partial^2 C}{\partial y^2}\right) + \frac{D_T}{T_\infty}\left(\frac{\partial^2 T}{\partial y^2}\right). \tag{4}$$

All parameters are specified in the Nomenclature section after to the conclusion, and the following CBCs pertain to this Scenario [22]:

$$-\kappa\left[\frac{\partial T}{\partial y}\right] = h_1\left(T_w - T\right), \qquad -D_B\left[\frac{\partial C}{\partial y}\right] = h_2\left(C_w - C\right), \qquad at \quad y = 0, \tag{5}$$

$$u = cx + \lambda_1\left[\frac{\partial u}{\partial y}\right], \qquad v = -v_w, \qquad at \quad y = 0, \tag{6}$$

$$u \to 0, \qquad T \to T_\infty, \qquad C \to C_\infty, \qquad as \quad y \quad \to \infty. \tag{7}$$

The equations have been made dimensionless with the introduction of particular normalized variables [18]:

$$\psi = \sqrt{c\nu}xf(\eta), \;\; \eta = \sqrt{\frac{c}{\nu}}y, \;\; \theta(\eta) = (T - T_\infty)(T_w - T_\infty)^{-1}, \;\; \phi(\eta) = (C - C_\infty)(C_w - C_\infty)^{-1}. \tag{8}$$

In this context, $\theta(\eta)$ represents the non-dimensionalized temperature, and $\phi(\eta)$ denotes the concentration in dimensionless form. Upon employing these variables (8), the governing equations for the BL equations (2)-(4) can be given in a non-dimensionalized form as follows:

$$\frac{d^3f}{d\eta^3} + f\frac{d^2f}{d\eta^2} - \left(\frac{df}{d\eta}\right)^2 - M\frac{df}{d\eta} = 0, \tag{9}$$

$$\frac{1}{Pr}(1+R)\frac{d^2\theta}{d\eta^2} + f\frac{d\theta}{d\eta} + \beta_b\left(\frac{d\theta}{d\eta}\frac{d\phi}{d\eta}\right) + \beta_t\left(\frac{d\theta}{d\eta}\right)^2 + Ec\left(\frac{d^2f}{d\eta^2}\right)^2 = 0, \tag{10}$$

$$\frac{d^2\phi}{d\eta^2} + Le\, f\frac{d\phi}{d\eta} + \frac{\beta_t}{\beta_b}\frac{d^2\theta}{d\eta^2} = 0. \tag{11}$$

Moreover, Subsequent to the application of the transformation, the CBCs assume the following formulation:

$$f(0) = f_w, \quad f'(0) = 1 + \lambda f''(0), \quad \theta'(0) = -Bi_1(1-\theta(0)), \quad \phi'(0) = -Bi_2(1-\phi(0)), \tag{12}$$

$$f'(\infty) \to 0, \qquad \theta(\infty) \to 0, \qquad \phi(\infty) \to 0. \tag{13}$$

All parameters are delineated in the nomenclature section following the conclusion.

The local skin-friction coefficient Cf_x, and the local Nusselt number Nu_x are delineated as the subsequent physical characteristics of interest:

$$Re_x^{\frac{1}{2}}Cf_x = -f''(0), \qquad Nu_xRe_x^{\frac{-1}{2}} = -\theta'(0), \qquad Sh_xRe_x^{\frac{-1}{2}} = -\phi'(0),$$

where $Re_x = \frac{u_w x}{\nu}$ is the local Reynolds number.

3. Procedure solution

3.1. Certain characteristics of the Hermite polynomials

Definition 1.

The Hermite polynomials (HPs) are defined by [11]:

$$H_n(\eta) = (-1)^n e^{\eta^2}\frac{d^n}{d\eta^n}e^{-\eta^2}, \qquad H_0(\eta) = 1, \quad H_1(\eta) = 2\eta, \quad H_2(\eta) = 4\eta^2 - 2.$$

The m-th derivatives of the HPs can be articulated by the subsequent relation:

$$H_n^{(m)}(\eta) = 2^m m!\begin{pmatrix} n \\ m \end{pmatrix} H_{n-m}(\eta) = \Delta_n^m H_{n-m}(\eta). \tag{14}$$

Now, to utilize these polynomials for function approximation, we shall define the following:

$$J_m = \text{span}\{H_0(\eta), H_1(\eta), ..., H_m(\eta)\}.$$

The $L^2_{w(\eta)}(\mathbb{R})$-orthogonal projection $\pi_m : L^2_{w(\eta)}(\mathbb{R}) \to J_m$ with respect to the weight function $w(\eta) = e^{-\eta^2}$, is given by:

$$\forall\ u(\eta) \in L^2_{w(\eta)}(\mathbb{R}) \text{ we have } < \pi_m(u(\eta)) - u(\eta), \psi(\eta) >= 0, \quad \forall\ \psi(\eta) \in J_m.$$

Utilizing the orthogonality property, we can now present the following approximation:

$$\pi_m(u) = \sum_{i=0}^{m-1} c_i H_i(\eta), \qquad c_i = \frac{1}{\sqrt{\pi} 2^i i!} < u(\eta), H_i(\eta) >_{L^2_{w(\eta)}(\mathbb{R})}, \qquad i = 0, 1, ..., m-1.$$

The function $\pi_m(u)$ is referred to as the Hermite expansion of $u(\eta)$ and serves as an approximation of $u(\eta)$ across $\mathbb{R}$ in most of the literature concerning spectral approaches. The HCM is utilized to numerically address various issues, including linear complex DEs [2] and linear DEs with variable coefficients [4]. For additional information regarding this procedure, see ([3], [9]).

3.2. Numerical implementation of the Hermite collocation method

To employ the HCM for resolving the proposed system (9)-(13) inside the domain $(0, \eta_\infty)$, where $\eta_\infty = 8$, we estimate $f(\eta)$, $\theta(\eta)$, and $\phi(\eta)$ as follows:

$$f(\eta) \simeq \sum_{\ell=0}^{m} a_\ell\, H_\ell(\eta), \qquad \theta(\eta) \simeq \sum_{\ell=0}^{m} b_\ell\, H_\ell(\eta), \qquad \phi(\eta) \simeq \sum_{\ell=0}^{m} c_\ell\, H_\ell(\eta). \tag{15}$$

Substitution from Eqs.(14), (15) in (9)-(11), we obtain:

$$\left(\sum_{\ell=3}^{m} a_\ell\, \Delta^3_\ell H_{\ell-3}(\eta)\right) + \left(\sum_{\ell=0}^{m} a_\ell\, H_\ell(\eta)\right)\left(\sum_{\ell=2}^{m} a_\ell\, \Delta^2_\ell H_{\ell-2}(\eta)\right) - \left(\sum_{\ell=1}^{m} a_\ell\, \Delta^1_\ell H_{\ell-1}(\eta)\right)^2 - M\left(\sum_{\ell=1}^{m} a_\ell\, \Delta^1_\ell H_{\ell-1}(\eta)\right) = 0, \tag{16}$$

$$\begin{aligned} &\frac{1}{Pr}(1+R)\left(\sum_{\ell=2}^{m} b_\ell\, \Delta^2_\ell H_{\ell-2}(\eta)\right) + \left(\sum_{\ell=0}^{m} a_\ell\, H_\ell(\eta)\right)\left(\sum_{\ell=1}^{m} b_\ell\, \Delta^1_\ell H_{\ell-1}(\eta)\right) \\ &+ \beta_b \left(\sum_{\ell=1}^{m} b_\ell\, \Delta^1_\ell H_{\ell-1}(\eta)\right)\left(\sum_{\ell=1}^{m} c_\ell\, \Delta^1_\ell H_{\ell-1}(\eta)\right) + \beta_t \left(\sum_{\ell=1}^{m} b_\ell\, \Delta^1_\ell H_{\ell-1}(\eta)\right)^2 \\ &+ Ec \left(\sum_{\ell=2}^{m} a_\ell\, \Delta^2_\ell H_{\ell-2}(\eta)\right)^2 = 0, \end{aligned} \tag{17}$$

$$\left(\sum_{\ell=2}^{m} c_\ell\, \Delta^2_\ell H_{\ell-2}(\eta)\right) + Le \left(\sum_{\ell=0}^{m} a_\ell\, H_\ell(\eta)\right)\left(\sum_{\ell=1}^{m} c_\ell\, \Delta^1_\ell H_{\ell-1}(\eta)\right) + \frac{\beta_t}{\beta_b}\left(\sum_{\ell=2}^{m} b_\ell\, \Delta^2_\ell H_{\ell-2}(\eta)\right) = 0. \tag{18}$$

We collocate Eq.(16) at $m-2$ nods $\eta_p, p=0,1,...,m-3$, and collocate Eqs.(17)-(18) at $m-1$ points $\eta_k, k=0,1,2,...,m-2$ as:

$$\left(\sum_{\ell=3}^{m} a_\ell\,\Delta_\ell^3 H_{\ell-3}(\eta_p)\right)+\left(\sum_{\ell=0}^{m} a_\ell\,H_\ell(\eta_p)\right)\left(\sum_{\ell=2}^{m} a_\ell\,\Delta_\ell^2 H_{\ell-2}(\eta_p)\right)-\left(\sum_{\ell=1}^{m} a_\ell\,\Delta_\ell^1 H_{\ell-1}(\eta_p)\right)^2 - M\left(\sum_{\ell=1}^{m} a_\ell\,\Delta_\ell^1 H_{\ell-1}(\eta_p)\right)=0, \tag{19}$$

$$\begin{aligned}&\frac{1}{Pr}(1+R)\left(\sum_{\ell=2}^{m} b_\ell\,\Delta_\ell^2 H_{\ell-2}(\eta_k)\right)+\left(\sum_{\ell=0}^{m} a_\ell\,H_\ell(\eta_k)\right)\left(\sum_{\ell=1}^{m} b_\ell\,\Delta_\ell^1 H_{\ell-1}(\eta_k)\right)\\ &+\beta_b\left(\sum_{\ell=1}^{m} b_\ell\,\Delta_\ell^1 H_{\ell-1}(\eta_k)\right)\left(\sum_{\ell=1}^{m} c_\ell\,\Delta_\ell^1 H_{\ell-1}(\eta_k)\right)+\beta_t\left(\sum_{\ell=1}^{m} b_\ell\,\Delta_\ell^1 H_{\ell-1}(\eta_k)\right)^2\\ &+Ec\left(\sum_{\ell=2}^{m} a_\ell\,\Delta_\ell^2 H_{\ell-2}(\eta_k)\right)^2=0,\end{aligned} \tag{20}$$

$$\begin{aligned}&\left(\sum_{\ell=2}^{m} c_\ell\,\Delta_\ell^2 H_{\ell-2}(\eta_k)\right)+Le\left(\sum_{\ell=0}^{m} a_\ell\,H_\ell(\eta_k)\right)\left(\sum_{\ell=1}^{m} c_\ell\,\Delta_\ell^1 H_{\ell-1}(\eta_k)\right)\\ &+\frac{\beta_t}{\beta_b}\left(\sum_{\ell=2}^{m} b_\ell\,\Delta_\ell^2 H_{\ell-2}(\eta_k)\right)=0.\end{aligned} \tag{21}$$

We utilize the roots of the Hermite polynomial $H_{m-1}(\eta)$ as appropriate collocation locations. Additionally, by putting Equation (15) into the CBCs (12)-(13), the following equations are derived:

$$\begin{aligned}&\sum_{\ell=0}^{m} H_\ell(0)\,a_\ell=f_w,\qquad \sum_{\ell=1}^{m}\Delta_\ell^1\,H_{\ell-1}(0)\,a_\ell-\lambda\left(\sum_{\ell=2}^{m}\Delta_\ell^2\,H_{\ell-2}(0)\,a_\ell\right)=1,\\ &\sum_{\ell=1}^{m}\Delta_\ell^1\,H_{\ell-1}(0)\,b_\ell+Bi_1\left(1-\sum_{\ell=0}^{m}H_\ell(0)\,b_\ell\right)=0,\\ &\sum_{\ell=1}^{m}\Delta_\ell^1\,H_{\ell-1}(0)\,c_\ell+Bi_2\left(1-\sum_{\ell=0}^{m}H_\ell(0)\,c_\ell\right)=0,\\ &\sum_{\ell=1}^{m}\Delta_\ell^1\,H_{\ell-1}(\eta_\infty)\,a_\ell=0,\qquad \sum_{\ell=0}^{m}H_\ell(\eta_\infty)\,b_\ell=0,\qquad \sum_{\ell=0}^{m}H_\ell(\eta_\infty)\,c_\ell=0.\end{aligned} \tag{22}$$

Equations (19)-(22) are a system of $(3m+3)$ nonlinear algebraic equations that may be solved using Newton iteration to determine coefficients a_i, b_i, and c_i for $i=0,1,2,...,m$. We can use formulas (15) to estimate the solution of the system (11)-(13).

4. Verification of the HCM

Now, the HCM was verified by comparing our results for assorted values of β_b with those reported in the prior study by Govardhan et al. [12]. This comparison has been reported in Table 1 when $f_w = M = \lambda = R = Ec = 0$, $Bi_1 \to 0$, $Bi_2 \to 0$ and $Pr = 10$, $\beta_t = 0.1$. This comparison revealed a strong agreement between the findings, affirming the accuracy and dependability of the HCM in representing the behavior of the studied system. The close alignment of both results supports the method's efficacy for this type of problem, highlighting its robustness for applications involving complex fluid dynamics.

Table 1. Comparison of $Re_x^{\frac{-1}{2}} Nu_x$ with the previous findings of Govardhan et al. [12] for assorted values of β_b when $f_w = M = \lambda = R = Ec = 0$, $Bi_1 \to 0$, $Bi_2 \to 0$ and $Pr = 10$, $\beta_t = 0.1$.

β_b	Govardhan et al. [12]	Present work
0.1	0.952376800	0.95237677951
0.2	0.693174600	0.69317459803
0.3	0.520079700	0.52007967980
0.4	0.402581500	0.40258149807
0.5	0.321055100	0.32105599085

5. Results and discussion

This section of the research presents the numerical results of the implementation of HCM. The study examined the effects of concentration, temperature, Eckert number, magnetic influence, suction, thermal radiation, and Brownian motion. This study examined their impact on velocity, concentration, and temperature parameters. Figure 2 shows how M affects $f'(\eta)$, $\phi(\eta)$, and $\theta(\eta)$. The graph shows how M affects these traits. The graphs demonstrate that a decrease in M results in a decrease in the velocity BL. Increasing temperature and concentration distributions slightly raises the magnetic parameter. The Lorentz force, which arises from the interaction of conductive fluids with magnetic fields, explains this. Our findings show that the Lorentz force reduces flow velocity. In a magnetic field, fluid particles resist more, raising the fluid's temperature. Additionally, previous studies by Dharmaiah and his colleagues ([7], [8]) highlight the impact of magnetic fields in fluid dynamics, especially in the context of nanofluid flow. Their findings reveal that magnetic fields play a critical role in controlling nanofluid movement and stability, influencing essential parameters such as flow rate, thermal transfer, and particle orientation within the fluid.

Figure 3 shows how the suction parameter f_w affects $f'(\eta)$, $\phi(\eta)$, and $\theta(\eta)$. This image shows how changes in the suction parameter affect the system's $f'(\eta)$, $\phi(\eta)$, and $\theta(\eta)$. The temperature, concentration, and velocity profiles fall significantly as suction increases. Suction on a stretching surface allows fluid migration, reducing BL thickness, velocity, temperature, and concentration distributions.The quantitative HCM results are reported

in this research section. The study examined concentration, temperature, Eckert number, magnetic influence, suction, thermal radiation, and Brownian motion as regulating elements. This study examined their effects on velocity, concentration, and temperature parameters. Figure 2 shows how M affects $f'(\eta)$, $\phi(\eta)$, and $\theta(\eta)$. The graph shows how M changes affect various properties. The graphs show that decreasing M lowers velocity BL. Increased temperature and concentration distributions increase magnetic parameter. This is explained by the Lorentz force, which occurs when conductive fluids interact with magnetic fields. Our findings show that the Lorentz force reduces flow velocity. In a magnetic field, fluid particles resist more, raising the fluid's temperature. The concentration of the nanofluid decreases as the suction parameter increases, owing to the enhanced removal of fluid particles from the BL. Through thinning the BL and limiting nanoparticle diffusion towards the surface, this increased suction lessens nanoparticle accumulation close to the surface, lowering the concentration profile in the nanofluid.

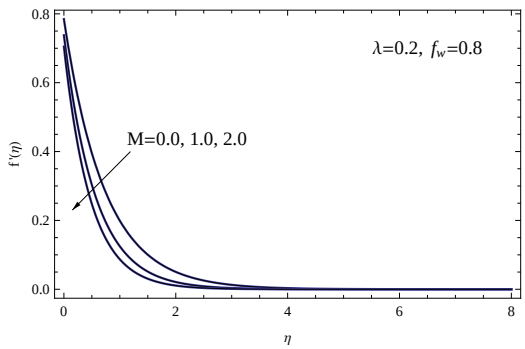

Figure 2. (a) $f'(\eta)$ for various M

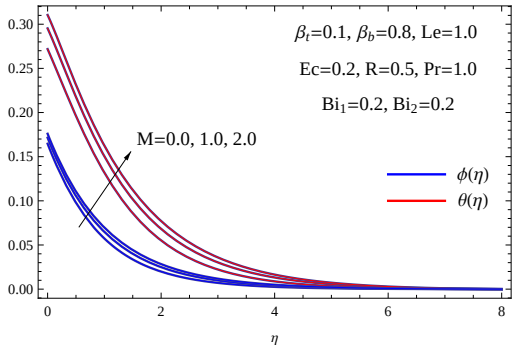

(b) $\phi(\eta)$ and $\theta(\eta)$ for various M

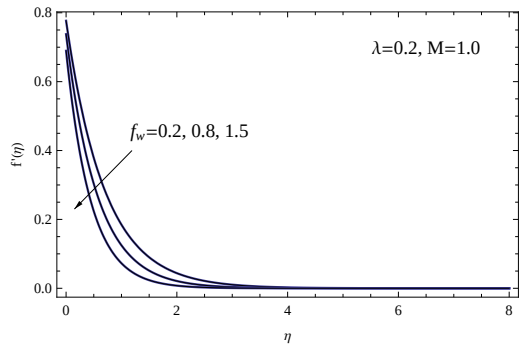

Figure 3. (a) $f'(\eta)$ for various f_w

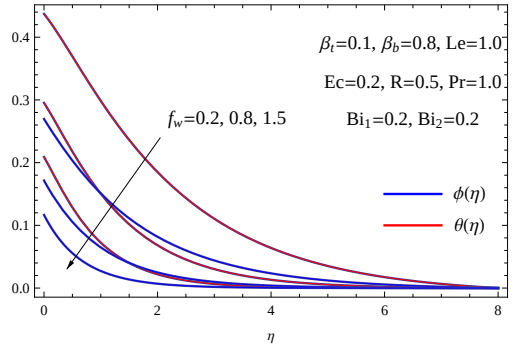

(b) $\phi(\eta)$ and $\theta(\eta)$ for various f_w

Figure 4 shows the impact of the slip parameter λ on the profiles of $f'(\eta)$, $\phi(\eta)$, and $\theta(\eta)$. Increased slip parameter improves concentration and temperature distributions. Additionally, the slip parameter is critical for velocity distribution obstruction. Physically, because a slip at the boundary lowers fluid-surface friction and slows the rate at which nanoparticles are removed from the BL, the concentration of nanofluid rises as the slip parameter increases. The total concentration within the BL rises as a result of the increased

ability of more nanoparticles to gather close to the surface due to the decreased shear. Further, the significance of the slip velocity phenomenon in fluid dynamics, particularly within the study of nanofluid flow, is underscored in prior research conducted by Jawad et al. [13]. Their work illustrates how slip velocity impacts flow behavior at the fluid-solid interface, influencing factors such as heat transfer efficiency, fluid resistance, and overall system performance.

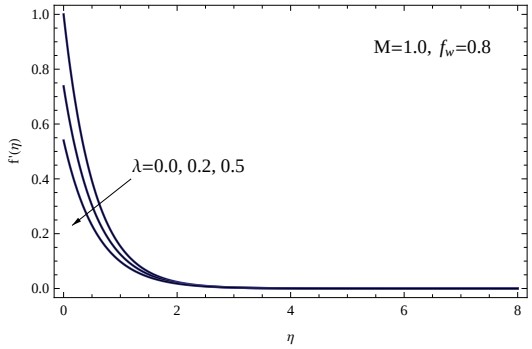

Figure 4. (a) $f'(\eta)$ for various λ

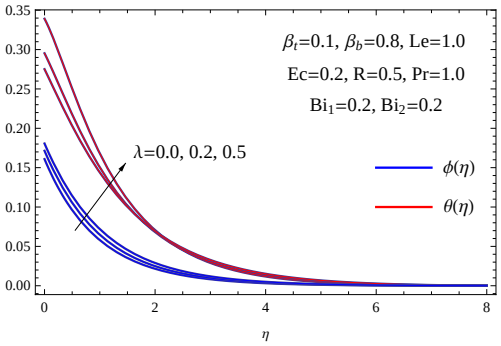

(b) $\phi(\eta)$ and $\theta(\eta)$ for various λ

Figure 5 shows the impact of Ec and R on $\theta(\eta)$. As Ec and R rise, thermal diffusion accelerates. Increasing both metrics directly affects the temperature profile. Furthermore, Ramesh and his colleagues' earlier study [20] emphasizes the role that heat radiation plays in nanofluid flow. Thermal radiation enhances energy transmission and influences fluid behavior near heated surfaces by having a considerable impact on the temperature distribution and heat transfer rates within the nanofluid, according to their findings. This effect is especially significant in applications that need effective thermal management because it improves stability and control over heat dissipation in systems that are subjected to high temperatures.

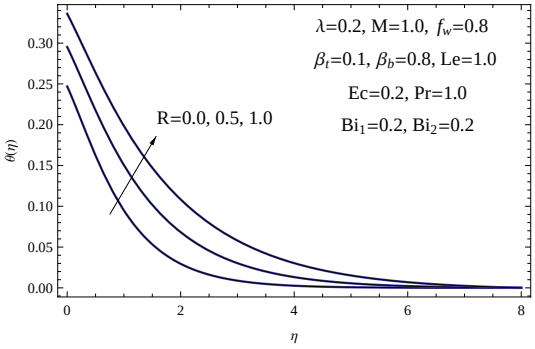

Figure 5. (a) $\theta(\eta)$ for various R

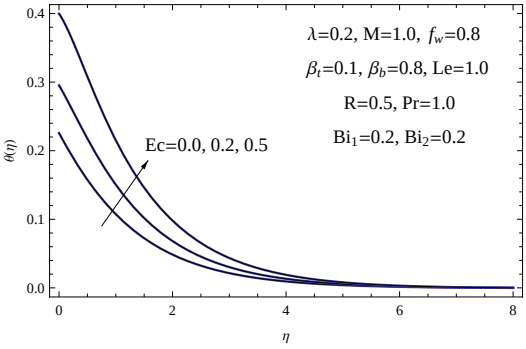

(b) $\theta(\eta)$ for various Ec

See Figure 6 for the impact of temperature and concentration Biot numbers on $\phi(\eta)$ and $\theta(\eta)$. The visualisation shows how Biot numbers affect system temperature and concentration spatially. Temperature and concentration dispersion increase proportionally

with thermal and concentration Biot numbers. An increase in heat transfer coefficient leads to higher values of Bi_1 and Bi_2, resulting in higher temperatures. Biot numbers must increase to improve thermal and concentration effects. Increased heat transfer coefficients raise system temperatures. A higher thermal Biot number increases convective heat transfer between the nanofluid and surface, raising its temperature. Improved convective heat transfer boosts the BL nanofluid temperature by increasing thermal energy transfer from the fluid's surface to the fluid.

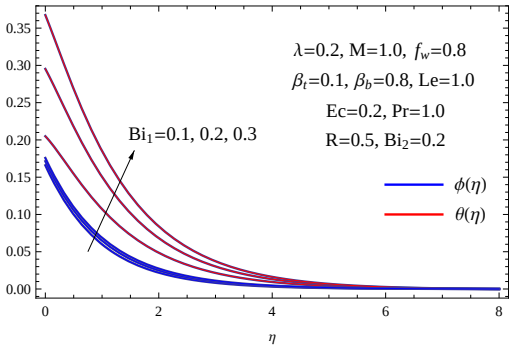

Figure 6. (a) $\phi(\eta)$ and $\theta(\eta)$ for various Bi_1

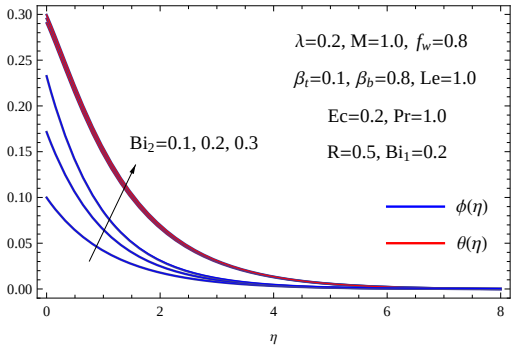

(b) $\phi(\eta)$ and $\theta(\eta)$ for various Bi_2

See Figure 7-a for the impact of β_t on $\phi(\eta)$ and $\theta(\eta)$ profiles. The graph shows how thermophoresis parameter changes affect system concentration and temperature. An increase in β_t broadens the concentration distribution and somewhat raises the temperature field. Nanoparticles are distributed by thermophoresis. See Figure 7-b for the impact of β_b on $\phi(\eta)$ and $\theta(\eta)$ profiles. As the Brownian motion parameter increases, the concentration distribution decreases and the temperature field barely rises. Physically, changing the Brownian motion parameter β_b can influence the random movement of nanoparticles in fluid, affecting their distribution and configuration. Higher Brownian motion nanoparticles have more kinetic energy and spread uniformly, whereas lower ones have less dispersive energy and may cluster or distribute unevenly.

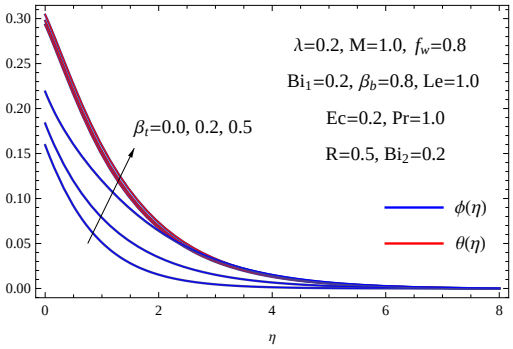

Figure 7. (a) $\phi(\eta)$ and $\theta(\eta)$ for various β_t

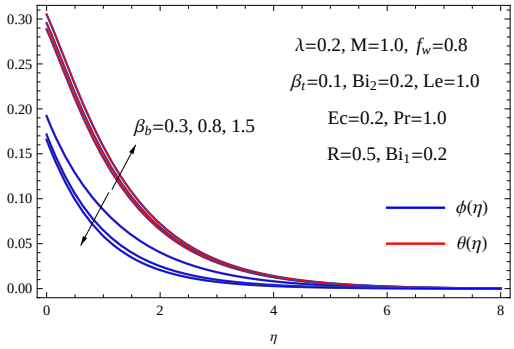

(b) $\phi(\eta)$ and $\theta(\eta)$ for various β_b

The drag force concept $\frac{Cf_x}{2}Re_x^{\frac{1}{2}}$ represents the resistance an item encounters in a fluid, such as gas or liquid. The object's speed and energy efficiency decrease as this force resists its travel through the medium. The Nusselt number $\frac{Nu_x}{\sqrt{Re_x}}$ is a key statistic for assessing convective heat transmission over a BL. It measures heat transfer between solid surfaces to reveal thermal interaction and heat dissipation efficiency. The Sherwood number $\frac{Sh_x}{\sqrt{Re_x}}$ measures the rate of material flow from a solid border to the surrounding fluid, indicating mass transfer efficiency in fluid flows. Studying molecule diffusion and substance dispersion in fluid media requires this dimensionless quantity. It evaluates mass transfer efficiency in industrial mixing, chemical processes, and environmental dispersion. Table 2 shows that increasing suction parameter values significantly increases Nusselt and Sherwood numbers. This implies faster heat and mass transmission. Additionally, increasing the suction parameter increases surface drag. However, as the magnetic field parameter increases, the Nusselt and Sherwood values decrease, indicating lower heat and mass transfer rates. The surface drag force increases, indicating that a higher magnetic field slows flow, influencing temperature and concentration BLs and increasing movement resistance. After careful investigation, the heat transfer coefficient falls as radiation, Eckert, and thermal Biot numbers rise. Increased thermal radiation, energy dissipation (Eckert number), and thermal BL effects (thermal Biot number) reduce heat transport. However, the heat transfer coefficient increases with the concentration Biot number, implying that increased mass transfer effects assist heat transfer. Raising the slip velocity parameter increases the Nusselt number, indicating better heat transfer efficiency, and reduces the drag force, showing reduced fluid flow resistance.

Table 2. Findings of $\frac{Cf_x}{2}Re_x^{\frac{1}{2}}$, $\frac{Nu_x}{\sqrt{Re_x}}$ and $\frac{Sh_x}{\sqrt{Re_x}}$ for various values of some controlling parameters with $Pr = Le = 1.0$

f_w	M	λ	Ec	R	β_t	β_b	Bi_1	Bi_2	$\frac{Cf_x}{2}Re_x^{\frac{1}{2}}$	$\frac{Nu_x}{\sqrt{Re_x}}$	$\frac{Sh_x}{\sqrt{Re_x}}$
0.2	1.0	0.2	0.2	0.5	0.1	0.8	0.2	0.2	1.1015487	0.5214785	0.1352895
0.8	1.0	0.2	0.2	0.5	0.1	0.8	0.2	0.2	1.2589301	0.6215874	0.1498520
1.5	1.0	0.2	0.2	0.5	0.1	0.8	0.2	0.2	1.5002589	0.7855201	0.1602547
0.8	0.0	0.2	0.2	0.5	0.1	0.8	0.2	0.2	0.9982018	0.8255202	0.1985412
0.8	1.0	0.2	0.2	0.5	0.1	0.8	0.2	0.2	1.2589301	0.6215874	0.1498520
0.8	2.0	0.2	0.2	0.5	0.1	0.8	0.2	0.2	1.5974521	0.7105587	0.1299987
0.8	1.0	0.0	0.2	0.5	0.1	0.8	0.2	0.2	1.4587412	0.4559852	0.1658952
0.8	1.0	0.2	0.2	0.5	0.1	0.8	0.2	0.2	1.2589301	0.6215874	0.1498520
0.8	1.0	0.5	0.2	0.5	0.1	0.8	0.2	0.2	1.1502587	0.7201455	0.1315873
0.8	1.0	0.2	0.0	0.5	0.1	0.8	0.2	0.2	1.2589301	0.6962301	0.1289620
0.8	1.0	0.2	0.2	0.5	0.1	0.8	0.2	0.2	1.2589301	0.6215874	0.1498520
0.8	1.0	0.2	0.5	0.5	0.1	0.8	0.2	0.2	1.2589301	0.5701852	0.1700369
0.8	1.0	0.2	0.2	0.0	0.1	0.8	0.2	0.2	1.2589301	0.7125896	0.1409852
0.8	1.0	0.2	0.2	0.5	0.1	0.8	0.2	0.2	1.2589301	0.6215874	0.1498520
0.8	1.0	0.2	0.2	1.0	0.1	0.8	0.2	0.2	1.2589301	0.5420589	0.1599802
0.8	1.0	0.2	0.2	0.5	0.0	0.8	0.2	0.2	1.2589301	0.6125896	0.1509851
0.8	1.0	0.2	0.2	0.5	0.2	0.8	0.2	0.2	1.2589301	0.5998521	0.1488514
0.8	1.0	0.2	0.2	0.5	0.5	0.8	0.2	0.2	1.2589301	0.5214789	0.1412016
0.8	1.0	0.2	0.2	0.5	0.1	0.3	0.2	0.2	1.2589301	0.6320158	0.1308753
0.8	1.0	0.2	0.2	0.5	0.1	0.8	0.2	0.2	1.2589301	0.6215874	0.1498520
0.8	1.0	0.2	0.2	0.5	0.1	1.5	0.2	0.2	1.2589301	0.6199875	0.1516789
0.8	1.0	0.2	0.2	0.5	0.1	0.8	0.1	0.2	1.2589301	0.5998740	0.1508123
0.8	1.0	0.2	0.2	0.5	0.1	0.8	0.2	0.2	1.2589301	0.6215874	0.1498520
0.8	1.0	0.2	0.2	0.5	0.1	0.8	0.3	0.2	1.2589301	0.6521092	0.1391572
0.8	1.0	0.2	0.2	0.5	0.1	0.8	0.2	0.1	1.2589301	0.6239980	0.1198540
0.8	1.0	0.2	0.2	0.5	0.1	0.8	0.2	0.2	1.2589301	0.6215874	0.1498520
0.8	1.0	0.2	0.2	0.5	0.1	0.8	0.2	0.3	1.2589301	0.6201925	0.1615973

Nomenclature

B_0	Strength of magnetic field
Bi_1, Bi_2	Thermal and Concentration Biot numbers
c	Constant related to stretching rate
C	Fluid concentration
c_p	Temperature buffering capacity
C_w	Nanoparticle density across the sheet
C_∞	Nanoparticle density at infinity
D_B	Random particle dispersal coefficient
D_T	Thermally induced migration rate
Ec	Dissipative heat parameter

f_w	The factor at which a fluid is absorbed
H_1, H_2	Thermal and Concentration convection coefficients
H_n	Hermite polynomials
Le	Lewis number
M	Magnetic field impact measure
q_r	Radiant heat transfer intensity
R	Radiation emission factor
Pr	Prandtl number
T	Internal fluid temperature
T_w	Heat level at the sheet's edge
Sh_x	Sherwood number
T_∞	Heat level away the sheet
v_w	Proportional suction rate
u_w	Expansion speed
x, y	$X - Y$ coordinate system

Greek symbols

λ	Slip parameter
μ	Viscosity
ϕ	Unitless concentration
κ	Thermal transmission capability
θ	Unitless temperature
ψ	Stream function
β_b	Brownian motion parameter
ρ	Density
β_t	Thermophoresis parameter
ν	Kinematic viscosity

6. Conclusions

This study examines the flow characteristics of MHD nanofluid over a stretched sheet, incorporating BL conditions. The investigation examined suction velocities, thermal radiation, viscous dissipation, and slip conditions. We applied a similarity transformation to reduce the problem's equations to ODEs. We used the Hermite collocation approach to quantitatively solve the problem. Outcomes of the inquiry.

As suction intensifies, temperature and concentration profiles diminish concurrently with velocity. An increase in a significant thermophoretic parameter elevates the concentration profile and marginally enhances the temperature field. As M increases, the temperature and concentration profiles elevate while the BL thickness diminishes. Temperature increases due to thermal radiation and viscous dissipation. As the slip velocity parameter increases, the profiles of $\phi(\eta)$ and $\theta(\eta)$ expand while the velocity field associated with the same value diminishes.

Acknowledgements

The researchers wish to extend their sincere gratitude to the Deanship of Scientific Research at the Islamic University of Madinah for the support provided to the Post-Publishing Program.

References

[1] W. Abbas, A. M. Megahed, M. A. Ibrahim, and A. A. M. Said. Ohmic dissipation impact on the flow of casson-williamson fluid over a slippery surface through a porous medium. *Indian Journal of Physics*, 12:1–7, 2023.

[2] M. Bagherpoorfard and F. A. Ghassabzade. Hermite matrix polynomial collocation method for linear complex differential equations and some comparisons. *J. of Applied Mathematics and Physics*, 1:58–64, 2013.

[3] B. Bialecki. A fast domain decomposition poisson solver on a rectangle for hermite bicubic orthogonal spline collocation. *Siam Journal Numerical Analysis*, 30:425–434, 1993.

[4] Z. K. Bojdi, S. Ahmadi-Asl, and A. Aminataei. Operational matrices with respect to hermite polynomials and their applications in solving linear differential equations with variable coefficients. *Journal of Linear and Topological Algebra*, 2:91–103, 2013.

[5] S. U. S. Choi. Enhancing thermal conductivity of fluids with nanoparticles. *Proceedings of the ASME International Mechanical Engineering Congress and Exposition*, 66:99–105, 1995.

[6] L. J. Crane. Flow past a stretching plate. *J. of Applied Mathematics and Physics*, 21:645–647, 1970.

[7] G. Dharmaiah, M. O. Fateh, K. S. Balamurugan, and N. Vedavathi. Numerical analysis of the magnetic dipole effect on a radiative ferromagnetic liquid flowing over a porous stretched sheet. *Fluid Dynamics & Materials Processing*, 31:1–22, 2023.

[8] G. Dharmaiah, M. O. Fateh, P. J. L. Rama, and B. Ch. Rani. Exploration of bio-convection for slippery two-phase maxwell nanofluid past a vertical induced magnetic stretching regime associated with biotechnology and engineering. *Journal of Molecular Liquids*, 391:123408, 2023.

[9] W. R. Dyksen and R. E. Lynch. A new decoupling technique for the hermite cubic collocation equations arising from boundary value problems. *Math. Comput. Simul.*, 54:359–372, 2000.

[10] M. O. Fateh, G. Dharmaiah, K. S. Balamurugan, A. I. Ismail, and S. Hemlata. The role of quadratic-linearly radiating heat source with carreau nanofluid and exponential space-dependent past a cone and a wedge: A medical engineering application and renewable energy. *Journal of Computational Biophysics and Chemistry*, 22:1–18, 2023.

[11] D. Funaro. *Polynomial Approximations of Differential Equations*. Springer-Verlag, 1992.

[12] K. Govardhan, G. Narender, and G. S. Sarma. Heat and mass transfer in mhd

nanofluid over a stretching surface along with viscous dissipation effect. *Int. J. Math. Eng. Manag. Sci.*, 5:343–352, 2020.

[13] R. Jawad, M. O. Fateh, A. Haider, and I. E. Sarris. Slip effects on casson nanofluid over a stretching sheet with activation energy: Rsm analysis. *Frontiers in Heat & Mass Transfer*, 22:1017–1041, 2024.

[14] M. M. Khader. Generalized fractional-order legendre polynomials and its treatment for solving system of fdes. *Indian Journal of Physics*, 96:3239–3246, 2022.

[15] M. M. Khader, Hijaz Ahmad, and A. M. Megahed. Developing some of engineering applications through numerical treatment of non-newtonian nanofluid flow on non-linear stretching surface with heat generation. *Case Studies in Thermal Engineering*, 51:1–12, 2023.

[16] M. M. Khader and M. M. Babatin. Hermite collocation method for obtaining the chaotic behavior of a non-linear coupled system of fdes. *International Journal of Modern Physics C*, 31:1–11, 2020.

[17] M. M. Khader, M. M. Babatin, and A. M. Megahed. On the numerical evaluation for studying ohmic dissipation and thermal conductivity impacts on the flow of casson fluid. *Case Studies in Thermal Engineering*, 49:1–10, 2023.

[18] A. M. Megahed. Improvement of heat transfer mechanism through a maxwell fluid flow over a stretching sheet embedded in a porous medium and convectively heated. *Mathematics and Computers in Simulation*, 187:97–109, 2021.

[19] G. Narender, G. Sreedhar, G. Sarma, and K. Govardhan. Heat and mass transfer of a nanofluid over a stretching sheet with viscous dissipation effect. *J. of Heat Mass Transfer Research*, 6:117–124, 2019.

[20] K. Ramesh, M. O. Fateh, A. I. Ismail, B. R. Jaiswal, A. S. Warke, R. K. Lodhi, and T. Sharma. Computational analysis on radiative non-newtonian carreau nanofluid flow in a microchannel under magnetic properties. *Scientia Iranica B*, 30:376–390, 2023.

[21] K. Ramesh, M. O. Fateh, and B. Souayeh. *Mathematical Modelling of Fluid Dynamics and Nanofluids*. CRC Press, Boca Raton, 2023.

[22] B. Srisailam, K. S. Reddy, G. Narender, and B. S. Malga. Flow and heat transfer analysis mhd nanofluid due to convective stretching sheet. *Indian J. Sci. Technol.*, 15:2393–2402, 2022.

[23] G. Thirupathi, K. Govardhan, and G. Narender. Viscous dissipation and radiative effects in the magneto-micropolar fluid with partial slip and convective boundary condition. *Surveys in Mathematics and its Applications*, 17:99–111, 2022.